Electronic Supplementary Information

Merging photoinitiated bulk polymerization and dopant-matrix design strategy for polymer-based organic afterglow materials

Xiuzheng Chen,[a,b] *Guangming Wang,*[b] *Minjian Wu,*[b] *Jiahui Liu,*[b] *Zhaohong Liu,*[*a] *Xuepu Wang,*[*b] *Yunlong Zou*[*b] *and Kaka Zhang*[*b]

[a.] Department of Chemistry, Northeast Normal University, Changchun 130024, China.
[b.] Key Laboratory of Synthetic and Self-Assembly Chemistry for Organic Functional Molecules, Shanghai Institute of Organic Chemistry, University of Chinese Academy of Sciences, Chinese Academy of Sciences, 345 Lingling Road, Shanghai 200032, People's Republic of China

*Email: liuzh944@nenu.edu.cn; wangxuepu@sioc.ac.cn; zouyunlong@sioc.ac.cn; zhangkaka@sioc.ac.cn

Table of Contents

Figure S19. (A) Room-temperature fluorescence spectra of spiroBF_2-PS samples. (B) Room-temperature phosphorescence spectra of spiroBF_2-PS samples.

Figure S20. (A) Room-temperature fluorescence spectra of spiroBF_2-PHEMA samples. (B) Room-temperature phosphorescence spectra of spiroBF_2-PHEMA samples.

Figure S21. (A) Room-temperature fluorescence spectra of fluoreneBF_2-PMMA samples. (B) Room-temperature phosphorescence spectra of fluoreneBF_2-PMMA samples.

Figure S22. (A) Room-temperature fluorescence spectra of fluoreneBF_2-PAA samples. (B) Room-temperature phosphorescence spectra of fluoreneBF_2-PAA samples.

Figure S23. (A) Room-temperature fluorescence spectra of fluoreneBF_2-PS samples. (B) Room-temperature phosphorescence spectra of fluoreneBF_2-PS samples.

Figure S24. (A) Room-temperature fluorescence spectra of fluoreneBF_2-PHEMA samples. (B) Room-temperature phosphorescence spectra of fluoreneBF_2-PHEMA samples.

Figure S25. (A) Room-temperature emission decay of spiroBF_2-PMMA-0.125% samples excited at 368 nm and monitored at 514 nm. (B) Room-temperature emission decay of spiroBF_2-PMMA-0.25% samples excited at 365 nm and monitored at 515 nm. (C) Room-temperature emission decay of spiroBF_2-PMMA-0.5% samples excited at 371 nm and monitored at 517 nm. (D) Room-temperature emission decay of spiroBF_2-PMMA-1% samples excited at 376 nm and monitored at 524 nm.

Figure S26. (A) Room-temperature emission decay of spiroBF_2-PAA-0.125% samples excited at 412 nm and monitored at 537 nm. (B) Room-temperature emission decay of spiroBF_2-PAA-0.25% samples excited at 399 nm and monitored at 538 nm. (C) Room-temperature emission decay of spiroBF_2-PAA-0.5% samples excited at 381 nm and monitored at 535 nm. (D) Room-temperature emission decay of spiroBF_2-PAA-1% samples excited at 370 nm and monitored at 535 nm.

Figure S27. (A) Room-temperature emission decay of spiroBF_2-PS-0.125% samples excited at 328 nm and monitored at 510 nm. (B) Room-temperature emission decay of spiroBF_2-PS-0.25% samples excited at 361 nm and monitored at 512 nm. (C) Room-temperature emission decay of spiroBF_2-PS-0.5% samples excited at 356 nm and monitored at 514 nm. (D) Room-temperature emission decay of spiroBF_2-PS-1% samples excited at 373 nm and monitored at 515 nm.

Figure S28. (A) Room-temperature emission decay of spiroBF_2-PHEMA-0.125% samples excited at 369 nm and monitored at 519 nm. (B) Room-temperature emission decay of spiroBF_2-PHEMA-0.25% samples excited at 372 nm and monitored at 522 nm. (C) Room-temperature emission decay of spiroBF_2-PHEMA-0.5% samples excited at 395 nm and monitored at 534 nm. (D) Room-temperature emission decay of spiroBF_2-PHEMA-1% samples excited at 428 nm and monitored at 542 nm.

Figure S29. (A) Room-temperature emission decay of fluoreneBF_2-PMMA-0.125% samples excited at 387 nm and monitored at 525 nm. (B) Room-temperature emission decay of fluoreneBF_2-PMMA-0.25% samples excited at 388 nm and monitored at 525 nm. (C) Room-temperature emission decay of fluoreneBF_2-PMMA-0.5% samples excited at 387 nm and monitored at 532 nm. (D) Room-temperature emission decay of fluoreneBF_2-PMMA-1% samples excited at 384 nm and monitored at 530 nm.

Figure S30. (A) Room-temperature emission decay of fluoreneBF_2-PAA-0.125% samples excited at 371 nm and monitored at 525 nm. (B) Room-temperature emission decay of fluoreneBF_2-PAA-0.25% samples excited at 402 nm and monitored at 539 nm. (C) Room-temperature emission decay of fluoreneBF_2-PAA-0.5% samples excited at 398 nm and monitored at 530 nm.

Figure S31. (A) Room-temperature emission decay of fluoreneBF$_2$-PS-0.125% samples excited at 364 nm and monitored at 511 nm. (B) Room-temperature emission decay of fluoreneBF$_2$-PS-0.25% samples excited at 365 nm and monitored at 510 nm. (C) Room-temperature emission decay of fluoreneBF$_2$-PS-0.5% samples excited at 365 nm and monitored at 512 nm. (D) Room-temperature emission decay of fluoreneBF$_2$-PS-1% samples excited at 366 nm and monitored at 511 nm.

Figure S32. (A) Room-temperature emission decay of fluoreneBF$_2$-PHEMA-0.125% samples excited at 367 nm and monitored at 517 nm. (B) Room-temperature emission decay of fluoreneBF$_2$-PHEMA-0.25% samples excited at 374 nm and monitored at 519 nm. (C) Room-temperature emission decay of fluoreneBF$_2$-PHEMA-0.5% samples excited at 376 nm and monitored at 521 nm.

Figure S33. Photographs of (A) spiroBF$_2$-PMMA'-0.5% and (B) spiroBF$_2$-PS'-0.5% from commercial polymers prepared by solution casting technique under 365 nm UV lamp and after removal of UV lamp, and PMMA' (CM-211) and PS' (Mn=170,000) are commercially available.

Figure S34. (A) UV-Vis spectra of spiroBF$_2$-PMMA'-0.5%. (B) Excitation spectra of spiroBF$_2$-PMMA'-0.5%. (C) Room-temperature fluorescence and phosphorescence spectra of spiroBF$_2$-PMMA'-0.5%. (D) Room-temperature emission decay of spiroBF$_2$-PMMA'-0.5% excited at 370 nm and monitored at 527 nm.

Figure S35. (A) UV-Vis spectra of spiroBF$_2$-PS'-0.5% (B) Excitation spectra of spiroBF$_2$-PS'-0.5%. (C) Room-temperature fluorescence and phosphorescence spectra of spiroBF$_2$-PS'-0.5%. (D) Room-temperature emission decay of spiroBF$_2$-PS'-0.5% excited at 369 nm and monitored at 521 nm.

Figure S36. Dipole moments of spiroBF$_2$'s S_1 state, PMMA's repeating unit, and PS's repeating unit.

Figure S37. Room-temperature emission decay of spiroBF$_2$-PS-0.5% materials monitored at 428 nm.

Figure S38. Room-temperature emission decay of spiroBF$_2$-PMMA-0.5% materials monitored at 434 nm.

Figure S39. Room-temperature emission decay of spiroBF$_2$-PhB-0.5% materials monitored at 451 nm.

Figure S40. Room-temperature emission decay of spiroBF$_2$-BP-0.5% materials monitored at 465 nm.

Figure S41. ^{1}H NMR spectra of spiroBF$_2$-PMMA-0.5% materials.

Figure S42. (A) Room-temperature fluorescence and phosphorescence spectra of two samples of spiroBF$_2$-PMMA-0.5% with and without initiator in degassed conditions. (B) Room-temperature emission decay of two samples of spiroBF$_2$-PMMA-0.5% with and without initiator in degassed conditions (excited at 371 nm and monitored at 525 nm).

Figure S43. (A) Room-temperature fluorescence and phosphorescence spectra of spiroBF$_2$-PMMA-0.5% measured at ambient conditions and in degassed conditions. (B) Room-temperature emission decay of spiroBF$_2$-PMMA-0.5% measured at ambient conditions and in degassed conditions; the former is excited by 367 nm and monitored by 515 nm, while the latter is excited by 375 nm and monitored by 522 nm.

Figure S44. (A) Room-temperature fluorescence and phosphorescence spectra of spiroBF$_2$-PMMA-0.5% before and after thermal annealing. (B) Room-temperature emission decay of spiroBF$_2$-PMMA-0.5% before and after thermal annealing; the former is excited by 367 nm and monitored by 515 nm, while the latter is excited by 382 nm and monitored by 523 nm.

Figure S45. (A) Room-temperature fluorescence and phosphorescence spectra on both sides of spiroBF_2-PMMA-0.5%. (B) Room-temperature emission decay on both sides of spiroBF_2-PMMA-0.5% excited by 367 nm and monitored by 515 nm.

Table S1. Cartesian coordinates of the optimized ground-state geometry of spiroBF_2.

Table S2. Cartesian coordinates of the optimized ground-state geometry of fluoreneBF_2.

Supporting References

Experimental Section

Materials

9,9-Spirobifluorene (98%, Bide Pharmatech), 9,9-dimethyl-9H-Fluorene (99%, InnoChem), acetic anhydride (98.5%, Sinopharm Chemical Reagent), boron trifluoride etherate (98%, TCI), benzophenone (BP) (99%, Macklin), phenyl benzoate (99%, Energy Chemical), methyl methacrylate (99%, Adamas), acrylic acid (99%, Macklin), styrene (99%, Aladdin), 2-hydroxyethyl methacrylate (98%, Dibo), 2-hydroxy-2-methyl-1-phenyl-1-acetone (98%, Dibo) were used as received.

Synthesis of spiroBF_2 via cascade reaction

Into a round bottom flask were added 9,9′-spirobifluorene (500 mg, 1.1 mmol), acetic anhydride (5 mL) and boron trifluoride diethyl etherate (0.8 mL). The reaction mixture was heated to 60 °C and stirred for 5 h. Then the reaction was quenched by adding the reaction mixture dropwise into cold water. The precipitates were washed by water for three times and dried under vacuum. The crude product was purified by column chromatography over silica gel using petroleum ether/dichloromethane (1:1) as eluent to give yellow solids with an isolation yield of 53%. The spiroBF_2 was further purified by three cycles of recrystallization in spectroscopic grade dichloromethane/hexane. Single crystals of spiroBF_2 were also grown from spectroscopic grade dichloromethane/hexane (CCDC 2049502). The synthesis procedure is the same as our previous studies (Adv. Opt. Mater. 2021, 2101909 and Adv. Optical Mater. 2021, 9, 2100353). ^{1}H NMR (400 MHz, Chloroform-*d*, relative to Me_4Si /ppm) δ 8.16 (dd, *J* = 8.2, 1.7 Hz, 1H), 7.98 (d, *J* = 8.1 Hz, 1H), 7.93 (d, *J* = 7.7 Hz, 1H), 7.89 (d, *J* = 7.6 Hz, 2H), 7.46 – 7.38 (m, 3H), 7.36 (d, *J* = 1.8 Hz, 1H), 7.22 (td, *J* = 7.5, 1.2 Hz, 1H), 7.13 (td, *J* = 7.5, 1.1 Hz, 2H), 6.76 (d, *J* = 7.6 Hz, 1H), 6.69 (d, *J* = 7.6 Hz, 2H), 6.36 (s, 1H), 2.30 (s, 3H). ^{13}C NMR (100 MHz, Chloroform-*d*) δ 191.59, 182.29, 150.69, 149.91, 149.54, 147.30, 142.05, 139.80, 130.46, 130.29, 129.81, 128.41, 128.39, 128.26, 124.84, 124.50, 124.07, 121.58, 120.74, 120.52, 97.51, 65.96, 24.71. ^{19}F NMR (376 MHz, 298K, Chloroform-*d*, relative to $CFCl_3$ /ppm) δ -140.06 (20%), -140.13 (80%). ^{11}B NMR (128 MHz, Chloroform-*d*, 298 K, relative to $BF_3{\cdot}Et_2O$ /ppm) δ -0.07. FT-IR (KBr, cm^{-1}): ν 3062, 2952, 2923, 1605, 1540, 1489, 1447, 1426, 1384, 1335, 1282, 1204, 1165, 1102, 1054, 1003, 980, 898, 880, 841, 808, 781, 759, 738, 727, 664, 636, 619, 582, 488, 466, 421. LRMS, m/z 470.1. HRMS (positive ESI) m/z found (calcd for $C_{29}H_{19}O_2{}^{10}BF_2$+$Na^+$): 470.1371 (470.1375).

Synthesis of D-spiroBF_2 via cascade reaction

The undeuterated H-spiro (200 mg) was treated with 10% Pd on active carbon (150 mg) and D_2O (30 mL) in a 130 mL teflon-lined autoclave at 240 °C for 12 h. The internal pressure reached 4–5 MPa. The deuteration reaction was performed in a safe laboratory in our institute. After slowly cooling to room temperature, the reaction mixture was extracted by ethyl acetate. The crude organic layer was dried over Na_2SO_4, filtered and reduced under vacuum. The crude D-spiro was purified by column chromatography over silica. After rotary evaporation and vacuum drying, the purified D-spiro was obtained with a yield of 87%. The deuteration yield of spiro was estimated from ^{1}H NMR to be 97%. For the preparation of D-spiroBF_2, D-spiro (100 mg), deuterated acetic anhydride (0.5 mL) and boron trifluoride diethyl etherate (0.19 mL) were added into a round bottom flask. The

reaction mixture was heated to 60 °C and stirred for 5 h. Then the reaction was quenched by adding the reaction mixture dropwise into cold water. The precipitates were washed by water for three times and dried under vacuum. The crude product was purified by column chromatography over silica gel using petroleum ether/dichloromethane (1:2) as eluent to give yellow solids with an isolation yield of 73%. The D-spiroBF_2 was further purified by recrystallization in spectroscopic grade dichloromethane/hexane. The synthesis procedure is the same as our previous studies (Adv. Opt. Mater. 2021, 2101909).

Synthesis of fluoreneBF_2 via cascade reaction

Into a round bottom flask were added 9,9-dimethyl-9*H*-fluorene (300 mg, 0.9 mmol), acetic anhydride (5 mL) and boron trifluoride diethyl etherate (0.4 mL). The reaction mixture was heated to 60 °C and stirred for 4 h. Then the reaction was quenched by adding the reaction mixture dropwise into cold water. The precipitates were washed by water for three times and dried under vacuum. The crude product was purified by column chromatography over silica gel using petroleum ether/dichloromethane (1:1) as eluent to give yellow solids with an isolation yield of 50%. The fluoreneBF_2 was further purified by three cycles of recrystallization in spectroscopic grade dichloromethane/hexane. Single crystals of fluoreneBF_2 were also grown from spectroscopic grade dichloromethane/hexane (CCDC 2049504). The synthesis procedure is the same as our previous studies (Adv. Optical Mater. 2021, 9, 2100353). ^{1}H NMR (400 MHz, Chloroform-*d*, relative to Me_4Si /ppm) δ 8.17 (d, *J* = 1.7 Hz, 1H), 8.04 (dd, *J* = 8.1, 1.7 Hz, 1H), 7.88 – 7.75 (m, 2H), 7.53 – 7.36 (m, 3H), 6.63 (s, 1H), 2.43 (s, 3H), 1.54 (s, 6H). ^{13}C NMR (100 MHz, Chloroform-*d*) δ 191.28, 182.90, 155.35, 154.61, 147.23, 137.41, 129.77, 129.07, 127.66, 123.63, 123.16, 121.63, 120.55, 97.40, 47.35, 26.95, 24.83. ^{19}F NMR (376 MHz, 298K, Chloroform-*d*, relative to $CFCl_3$ /ppm) δ -139.08 (20%), -139.14 (80%). ^{11}B NMR (128 MHz, Chloroform-*d*, 298 K, relative to $BF_3{\cdot}Et_2O$ /ppm) δ 0.10. FT-IR (KBr, cm^{-1}): ν 2966, 2926, 2863, 1610, 1534, 1473, 1440, 1428, 1357, 1336, 1210, 1158, 1109, 1088, 1055, 1007, 978, 912, 828, 792, 776, 761, 736, 639, 585, 568, 488, 427. LRMS, m/z 348.1. HRMS (positive ESI) m/z found (calcd for $C_{19}H_{17}O_2{}^{10}BF_2{+}Na^+$): 348.1216 (348.1218).

Preparation of afterglow materials by merging photoinitiated bulk polymerization and dopant-matrix design strategy

We select photoinitiated bulk polymerization to convert monomers into polymers. 365 nm UV lamp (75 W) was used, and the distance from UV lamp to samples was fixed at 50 cm. By using 2-hydroxy-2-methyl-1-phenyl-1-acetone (HMPP) as photoinitiator, it was found that monomers such as methyl methacrylate (MMA), acrylic acid (AA), styrene (St), and 2-hydroxyethyl methacrylate (HEMA) became transparent solids after 365 nm UV irradiation for several hours. The obtained polymer solids showed insignificant organic afterglow under ambient conditions. Interestingly, after irradiating the solutions of monomers, HMPP and BF_2bdk for tens of minutes to several hours (please find the following table), the obtained solids were found to exhibit significant organic afterglow under ambient conditions. The layer of the liquid precursors has a thickness of around 3 mm for photopolymerization. Since the monomers have negligible absorption at 365 nm and the concentration of photoinitiators is as low as 0.2%, the UV light can penetrate the liquid precursors

to uniformly initiate the polymerization. It has been found that the top side and bottom side of the obtained BF_2bdk-polymer samples showed similar RTP properties (Figure S45).

Sample \ C / T	0.125%	0.25%	0.5%	1%
PHEMA-BF_2bdk	10 min	15 min	20 min	30 min
PMMA-BF_2bdk	20 min	30 min	40 min	50 min
PAA—BF_2bdk	20 min	30 min	50 min	70 min
PS-BF_2bdk	60 min	90 min	140 min	180 min

Physical measurements and instrumentation

^{1}H NMR (400 MHz), ^{13}C{^{1}H} NMR (100 MHz), ^{19}F NMR (376 MHz) and ^{11}B NMR (128 MHz) spectra were recorded on a JEOL Fourier-transform NMR spectrometer (400 MHz). Mass spectra were performed on Agilent Technologies 5973N and Thermo Fisher Scientific LTQ FT Ultras mass spectrometer. FT-IR spectra were recorded on a Nicolet AVATAR-360 FT-IR spectrophotomerter with a resolution of 4 cm^{-1}. UV-Vis absorption spectra were recorded on a Hitachi U-3310 UV-vis spectrophotometer and a Techcomp UV1050 UV-vis spectrophotometer. Emission spectra were recorded using Hitachi FL-7000 fluorescence spectrometer. Photoluminescence quantum yield was measured by a Hamamatsu absolute PL quantum yield measurement system based on a standard protocol. Photographs and videos were captured by iPhone12 cameras. Before imaging, samples were irradiated by a 365 nm UV lamp (75 W) for approximately 5 s at a distance of approximately 15 cm. Single-crystal X-ray diffraction analysis was performed on a D8 VENTURE SC-XRD instrument. The X-ray crystallographic data for spiroBF_2, fluoreneBF_2 has been deposited at the Cambridge Crystallographic Data Centre (CCDC), under the deposition number CCDC 2049502 (data_mo_d8v20638_0m) and 2049504 (data_mo_d8v20682_0m), respectively.

TD-DFT calculations

TD-DFT calculations were performed on ORCA 4.2.1 program with B3LYP functional and def2-TZVP(-f) basis set to study the photophysical properties of molecularly dispersed spiroBF_2 and fluoreneBF_2 in the solid state.[S1-S5] Spin-orbit coupling (SOC) matrix elements between the singlet excited states and triplet excited states were calculated with spin-orbit mean-field (SOMF) methods. Since the afterglow properties are originated from the excited states of molecularly dispersed BF_2bdk in the rigid matrices where intramolecular rotation and vibration are largely restricted, the optimized geometry of spiroBF_2 and fluoreneBF_2 ground state was used for all the TD-DFT calculations. It is found that the optimized geometry of BF_2bdk ground state is similar to the single crystal structure of spiroBF_2 and fluoreneBF_2. Electron density difference plots were analyzed by Multiwfn and rendered by VMD.[S6-S7]

Text S1. About the photophysical data in Table 1.

BF_2bdk molecules in PAA systems possess long RTP lifetimes because of the presence of strong hydrogen bonding with in PAA matrices which can largely suppress the nonradiative decay

of BF_2bdk molecules dispersed in the matrices. PHEMA systems showed relatively short RTP lifetimes, which can be explained by the relatively long side groups of PHEMA that may reduce the rigidity of the polymer matrices. The relatively short RTP lifetimes of PS systems can be attributed to the small dipole-dipole interactions between PS matrices and BF_2bdk's S_1 states. In the case of fluoreneBF_2-PMMA, the RTP lifetimes decrease with the increase of doping concentration. This can be attributed to aggregation-caused quenching of the planar fluoreneBF_2 molecules due to their poor solubility in PMMA. In the case of fluoreneBF_2-PS, there are non-covalent interactions between the aromatic groups of fluoreneBF_2 molecules and PS matrices, so the aggregation-caused quenching is insignificant in fluoreneBF_2-PS system upon increasing doping concentration. For the spiroBF_2-PS system, because of the relatively low RTP intensity, some quenching factors would have significant influence on RTP lifetimes of the samples at low doping concentrations. By increasing doping concentration, such influence would be reduced as can be seen from the compositions of shorter RTP lifetime components (Figure S27).

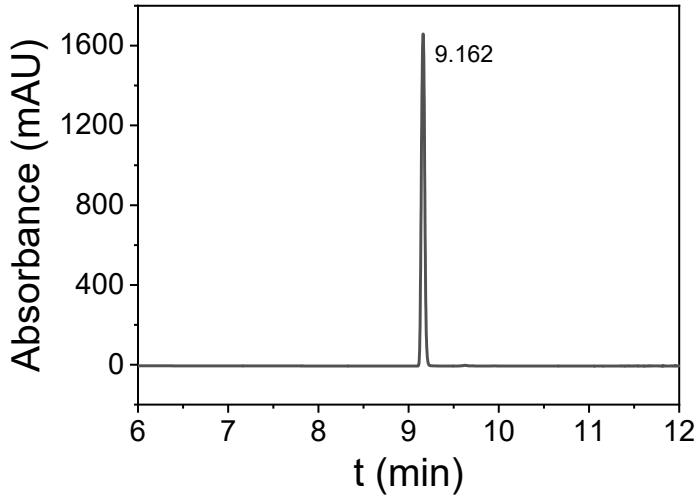

Figure S1. HPLC spectrum of spiroBF_2, monitored by UV detector at 380 nm.

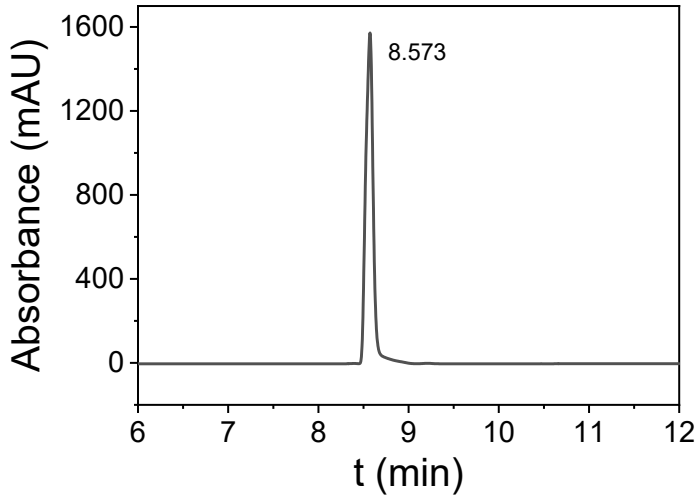

Figure S2. HPLC spectrum of fluoreneBF_2, monitored by UV detector at 376 nm.

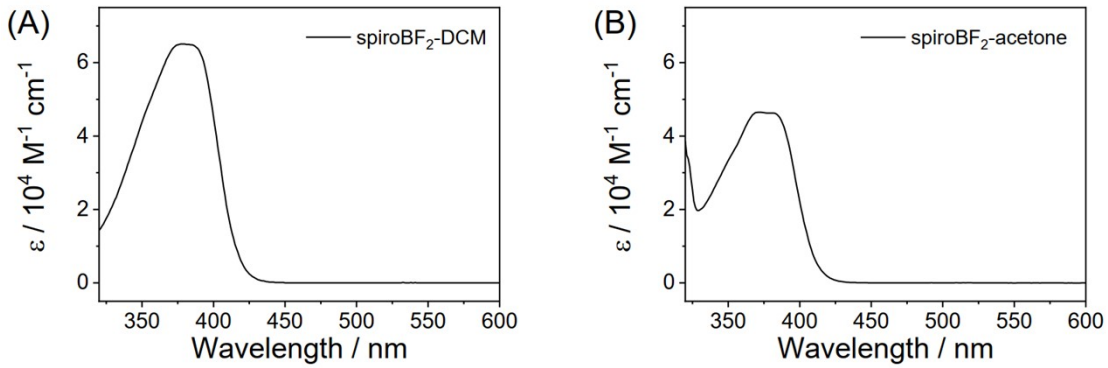

Figure S3. (A) UV-Vis spectra of spiroBF$_2$ in DCM. (B) UV-Vis spectra of spiroBF$_2$ in acetone.

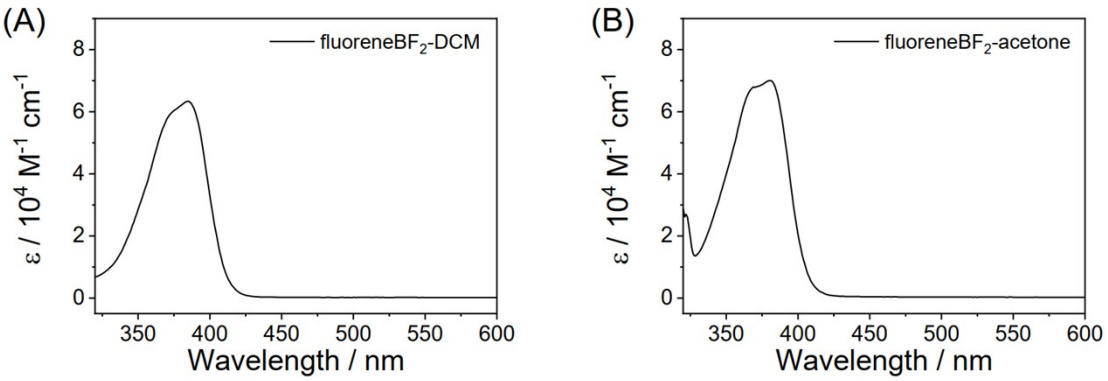

Figure S4. (A) UV-Vis spectra of fluoreneBF$_2$ in DCM. (B) UV-Vis spectra of fluoreneBF$_2$ in acetone.

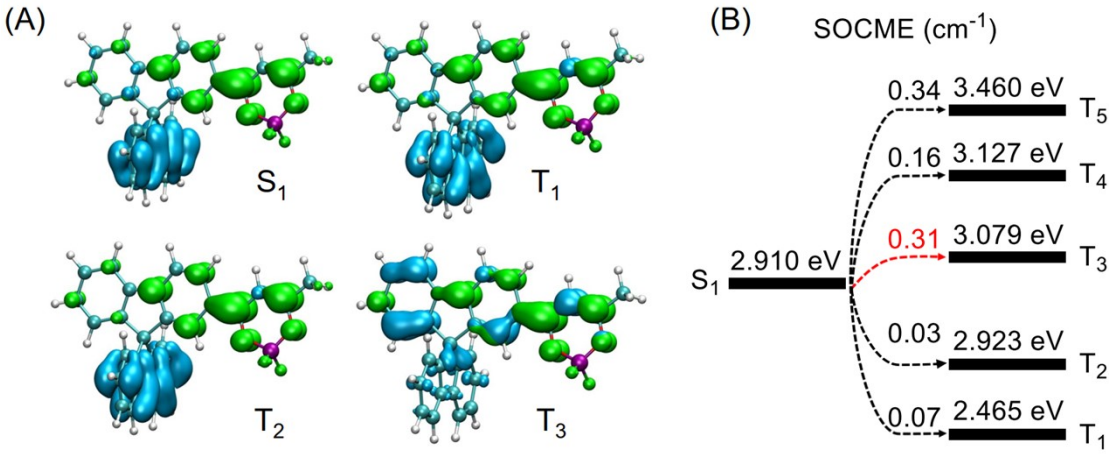

Figure S5. (A) The isosurface maps of spiroBF$_2$ singlet, the oscillator frequency and triplet excited states based on the TD-DFT calculated results. Blue and green isosurfaces correspond to hole and electron distributions, respectively. (B) TD-DFT calculated energy levels of spiroBF$_2$ singlet and triplet excited states and their spin-orbit coupling matrix elements (SOCME).

Figure S6. Photographs of PMMA, PAA, PS, PHEMA obtained by photoinitiated bulk polymerization without BF$_2$bdk addition under 365 nm UV lamp and after removal of UV lamp.

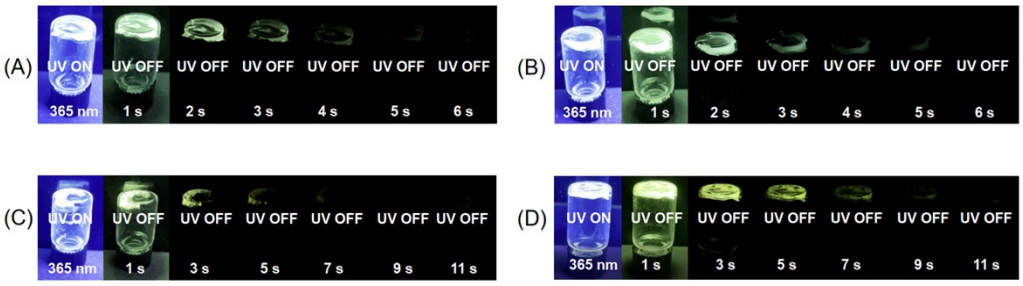

Figure S7. Photographs of (A) spiroBF$_2$-PMMA-0.125%, (B) spiroBF$_2$-PMMA-0.25%, (C) spiroBF$_2$-PMMA-0.5% and (D) spiroBF$_2$-PMMA-1% under 365 nm UV lamp and after removal of UV lamp.

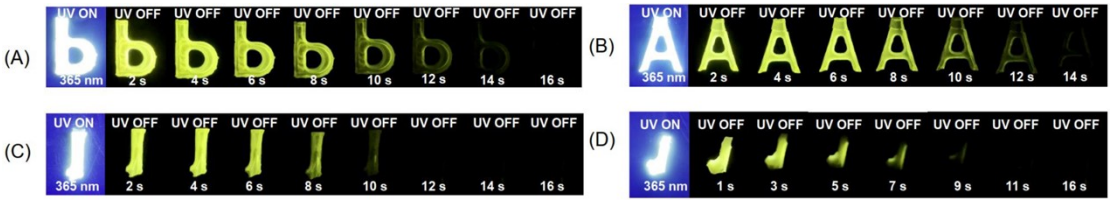

Figure S8. Photographs of (A) spiroBF$_2$-PAA-0.125%, (B) spiroBF$_2$-PAA-0.25%, (C) spiroBF$_2$-PAA-0.5% and (D) spiroBF$_2$-PAA-1% under 365 nm UV lamp and after removal of UV lamp.

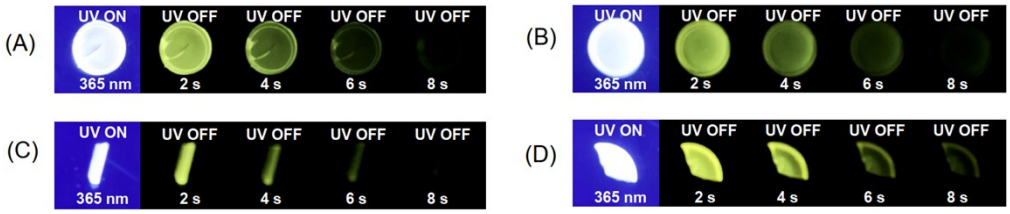

Figure S9. Photographs of (A) spiroBF$_2$-PS-0.125%, (B) spiroBF$_2$-PS-0.25%, (C) spiroBF$_2$-PS-0.5% and (D) spiroBF$_2$-PS-1% under 365 nm UV lamp and after removal of UV lamp.

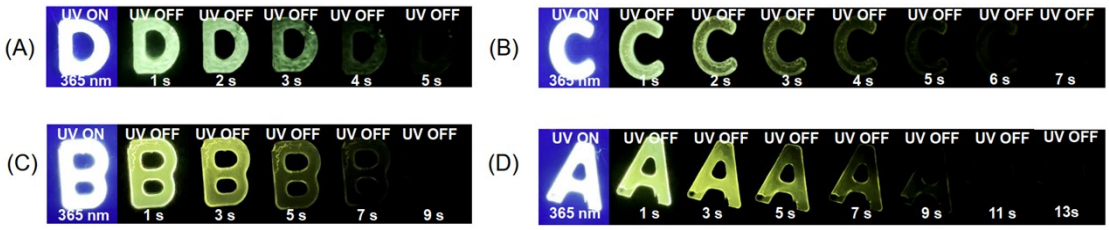

Figure S10. Photographs of (A) spiroBF$_2$-PHEMA-0.125%, (B) spiroBF$_2$-PHEMA-0.25%, (C) spiroBF$_2$-PHEMA-0.5% and (D) spiroBF$_2$-PHEMA-1% under 365 nm UV lamp and after removal of UV lamp.

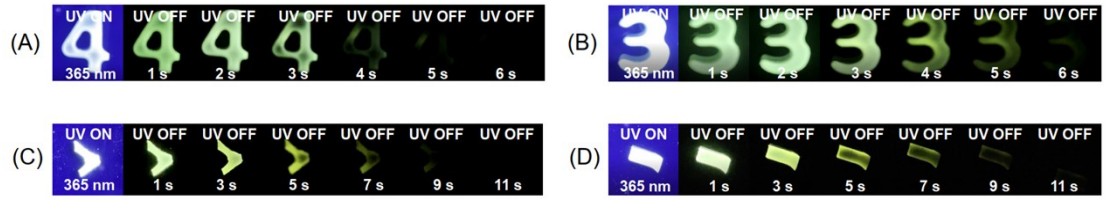

Figure S11. Photographs of (A) fluoreneBF$_2$-PMMA-0.125%, (B) fluoreneBF$_2$-PMMA-0.25%, (C) fluoreneBF$_2$-PMMA-0.5% and (D) fluoreneBF$_2$-PMMA-1% under 365 nm UV lamp and after removal of UV lamp.

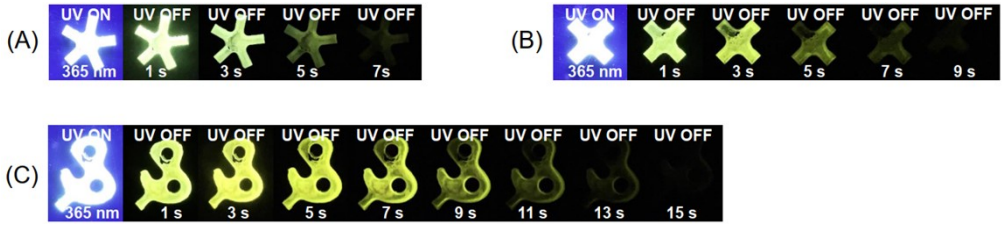

Figure S12. Photographs of (A) fluoreneBF$_2$-PAA-0.125%, (B) fluoreneBF$_2$-PAA-0.25%, (C) and fluoreneBF$_2$-PAA-0.5% under 365 nm UV lamp and after removal of UV lamp.

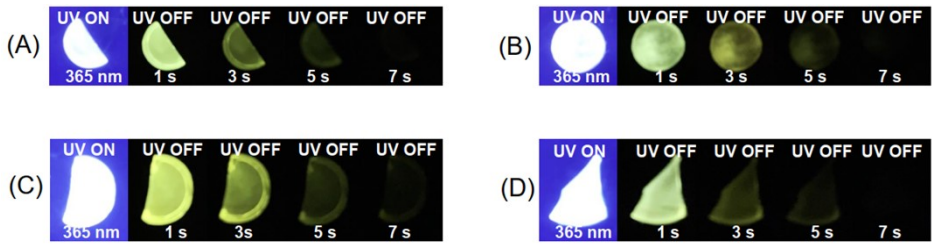

Figure S13. Photographs of (A) fluoreneBF$_2$-PS-0.125%, (B) fluoreneBF$_2$-PS-0.25%, (C) fluoreneBF$_2$-PS-0.5% and (D) fluoreneBF$_2$-PS-1% under 365 nm UV lamp and after removal of UV lamp.

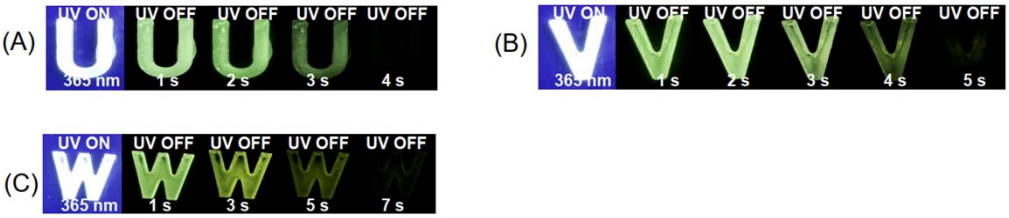

Figure S14. Photographs of (A) fluoreneBF$_2$-PHEMA-0.125%, (B) fluoreneBF$_2$-PHEMA-0.25%, and (C) fluoreneBF$_2$-PHEMA-0.5% under 365 nm UV lamp and after removal of UV lamp.

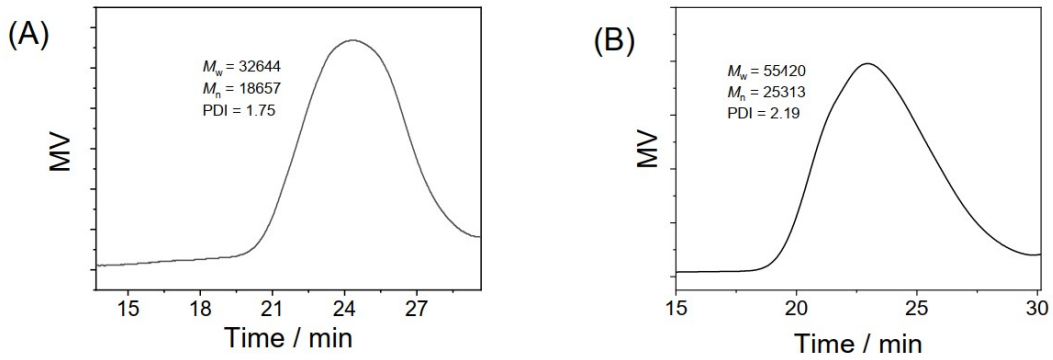

Figure S15. GPC profile of (A) PMMA and (B) PS after photopolymerization (THF phase, PS standard).

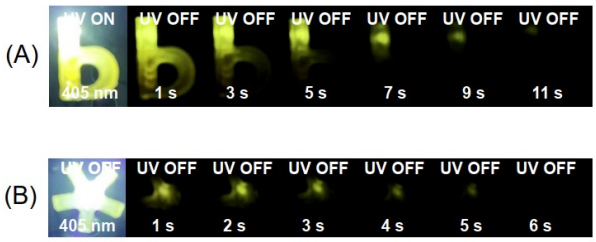

Figure S16. Photographs of (A) spiroBF$_2$-PAA-0.125% and (B) fluoreneBF$_2$-PAA-0.125% under 405 nm lamp and after removal of lamp.

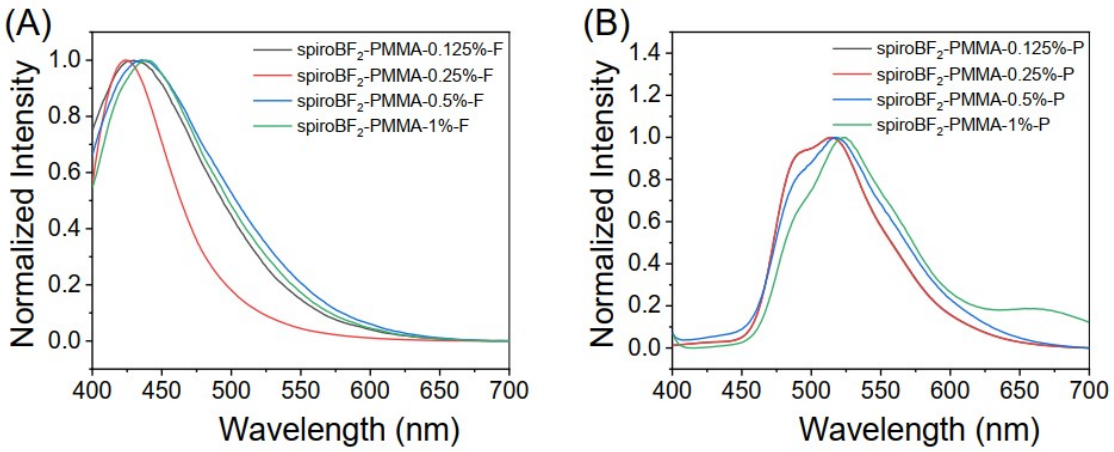

Figure S17. (A) Room-temperature fluorescence spectra of spiroBF$_2$-PMMA samples. (B) Room-temperature phosphorescence spectra of spiroBF$_2$-PMMA samples.

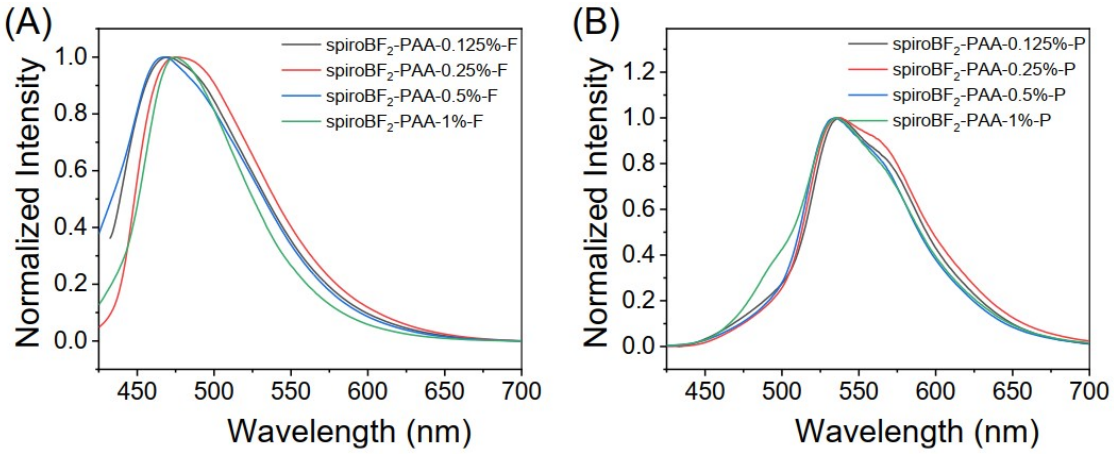

Figure S18. (A) Room-temperature fluorescence spectra of spiroBF$_2$-PAA samples. (B) Room-temperature phosphorescence spectra of spiroBF$_2$-PAA samples.

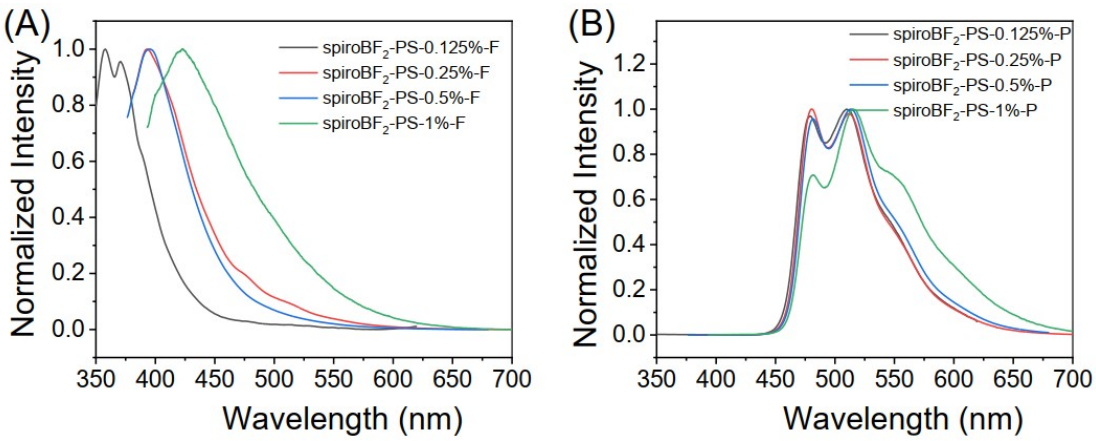

Figure S19. (A) Room-temperature fluorescence spectra of spiroBF$_2$-PS samples. (B) Room-temperature phosphorescence spectra of spiroBF$_2$-PS samples.

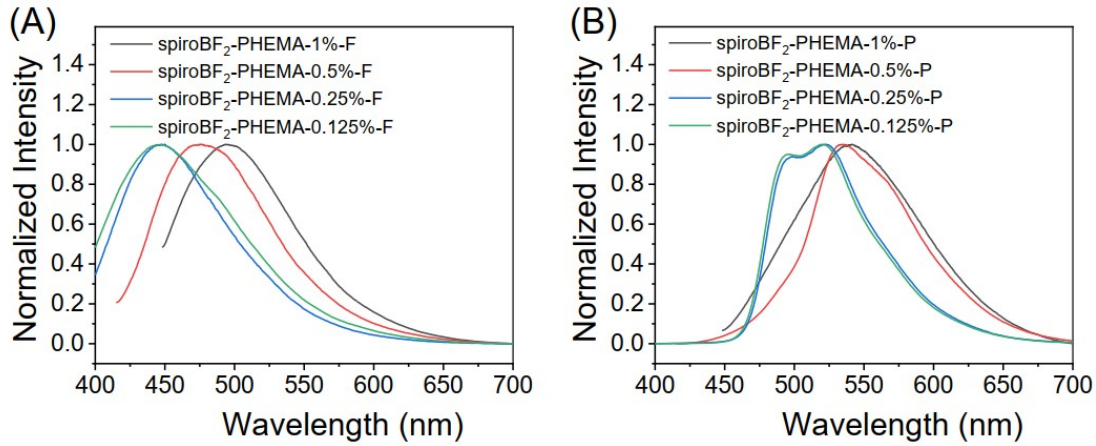

Figure S20. (A) Room-temperature fluorescence spectra of spiroBF$_2$-PHEMA samples. (B) Room-temperature phosphorescence spectra of spiroBF$_2$-PHEMA samples.

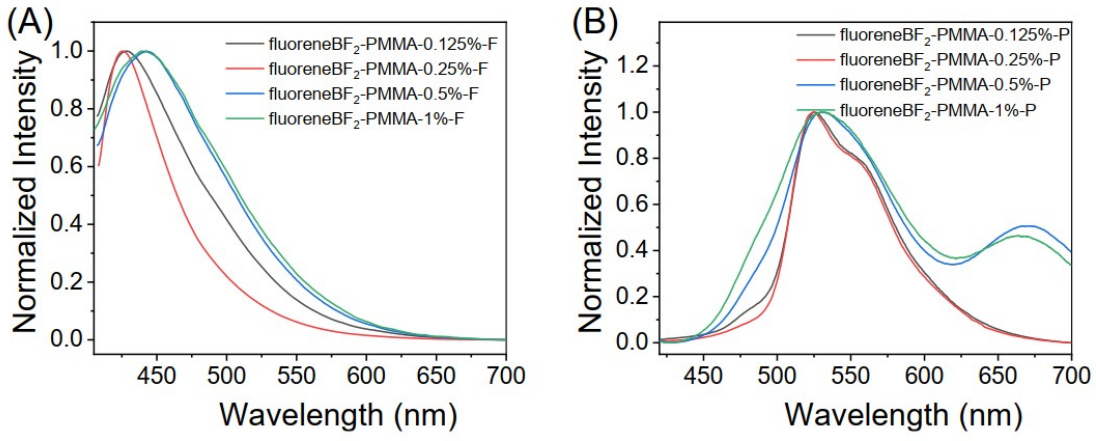

Figure S21. (A) Room-temperature fluorescence spectra of fluoreneBF$_2$-PMMA samples. (B) Room-temperature phosphorescence spectra of fluoreneBF$_2$-PMMA samples.

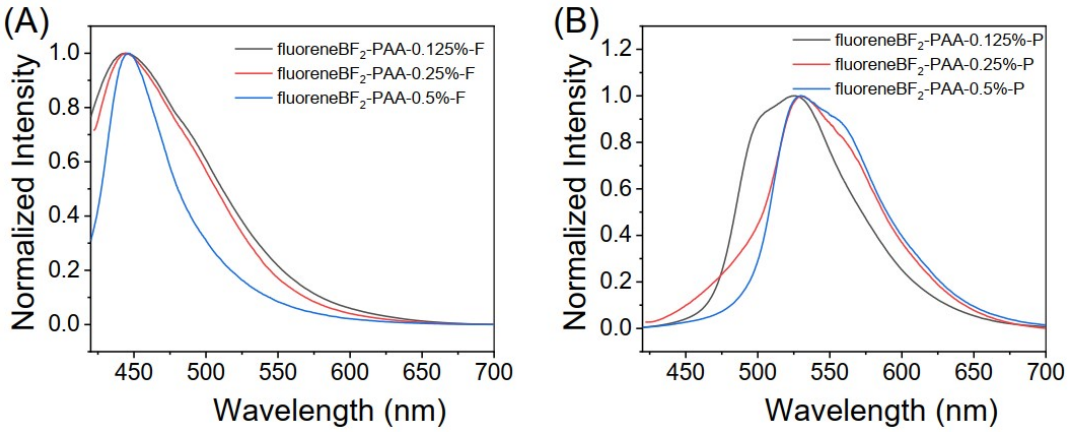

Figure S22. (A) Room-temperature fluorescence spectra of fluoreneBF$_2$-PAA samples. (B) Room-temperature phosphorescence spectra of fluoreneBF$_2$-PAA samples.

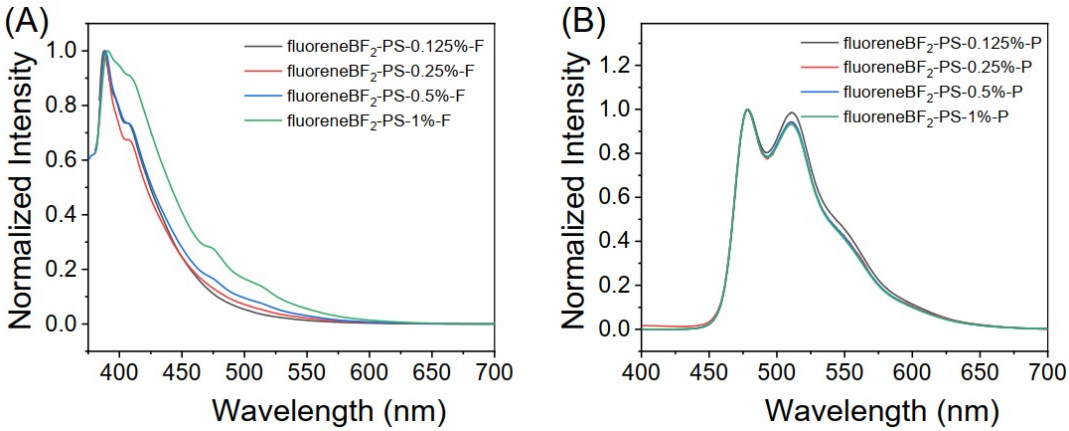

Figure S23. (A) Room-temperature fluorescence spectra of fluoreneBF$_2$-PS samples. (B) Room-temperature phosphorescence spectra of fluoreneBF$_2$-PS samples.

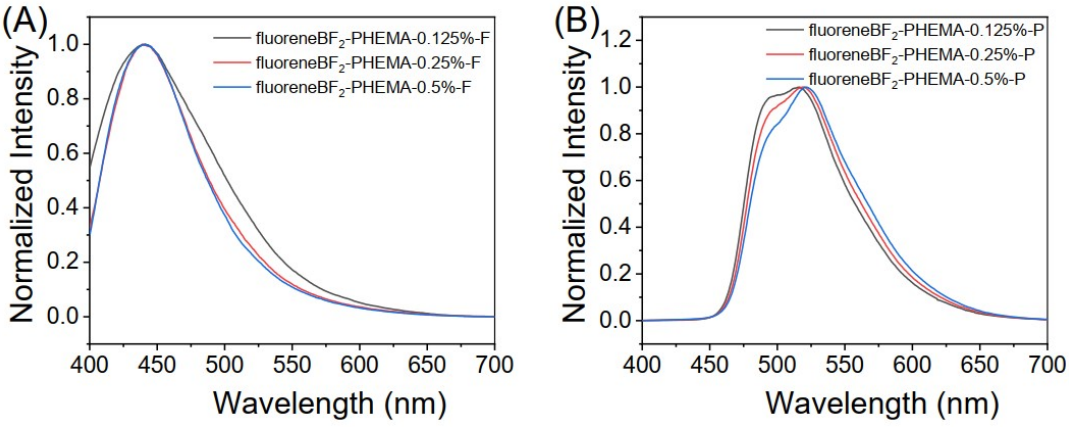

Figure S24. (A) Room-temperature fluorescence spectra of fluoreneBF$_2$-PHEMA samples. (B) Room-temperature phosphorescence spectra of fluoreneBF$_2$-PHEMA samples.

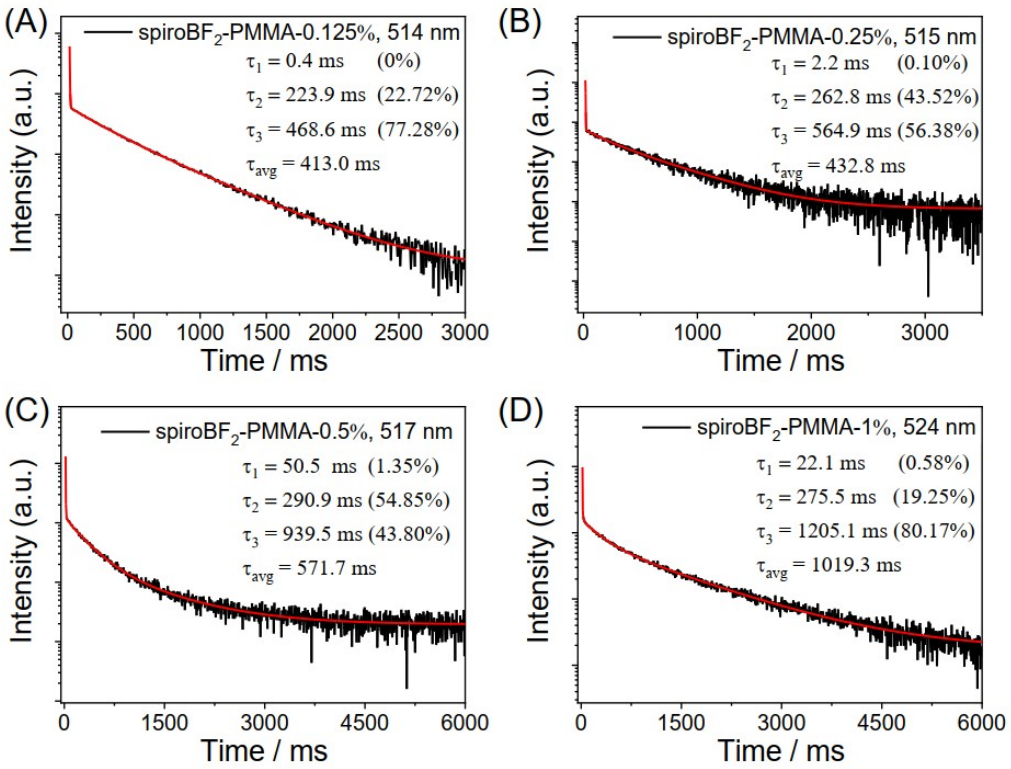

Figure S25. (A) Room-temperature emission decay of spiroBF$_2$-PMMA-0.125% samples excited at 368 nm and monitored at 514 nm. (B) Room-temperature emission decay of spiroBF$_2$-PMMA-0.25% samples excited at 365 nm and monitored at 515 nm. (C) Room-temperature emission decay of spiroBF$_2$-PMMA-0.5% samples excited at 371 nm and monitored at 517 nm. (D) Room-temperature emission decay of spiroBF$_2$-PMMA-1% samples excited at 376 nm and monitored at 524 nm.

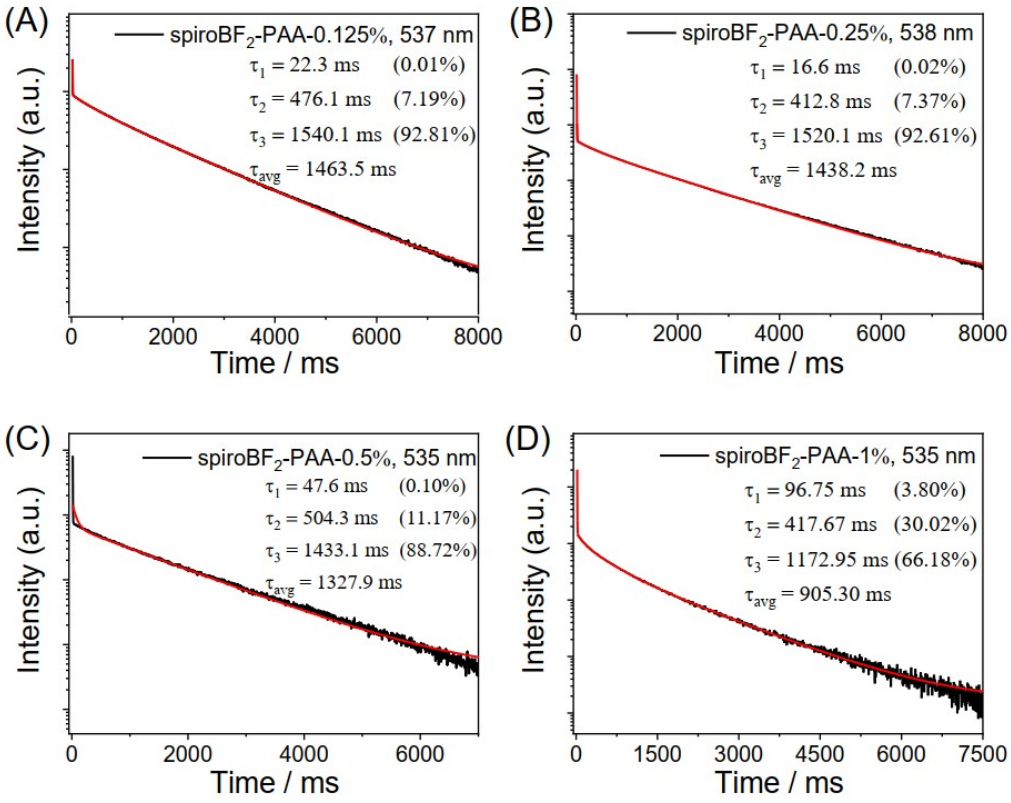

Figure S26. (A) Room-temperature emission decay of spiroBF$_2$-PAA-0.125% samples excited at 412 nm and monitored at 537 nm. (B) Room-temperature emission decay of spiroBF$_2$-PAA-0.25% samples excited at 399 nm and monitored at 538 nm. (C) Room-temperature emission decay of spiroBF$_2$-PAA-0.5% samples excited at 381 nm and monitored at 535 nm. (D) Room-temperature emission decay of spiroBF$_2$-PAA-1% samples excited at 370 nm and monitored at 535 nm.

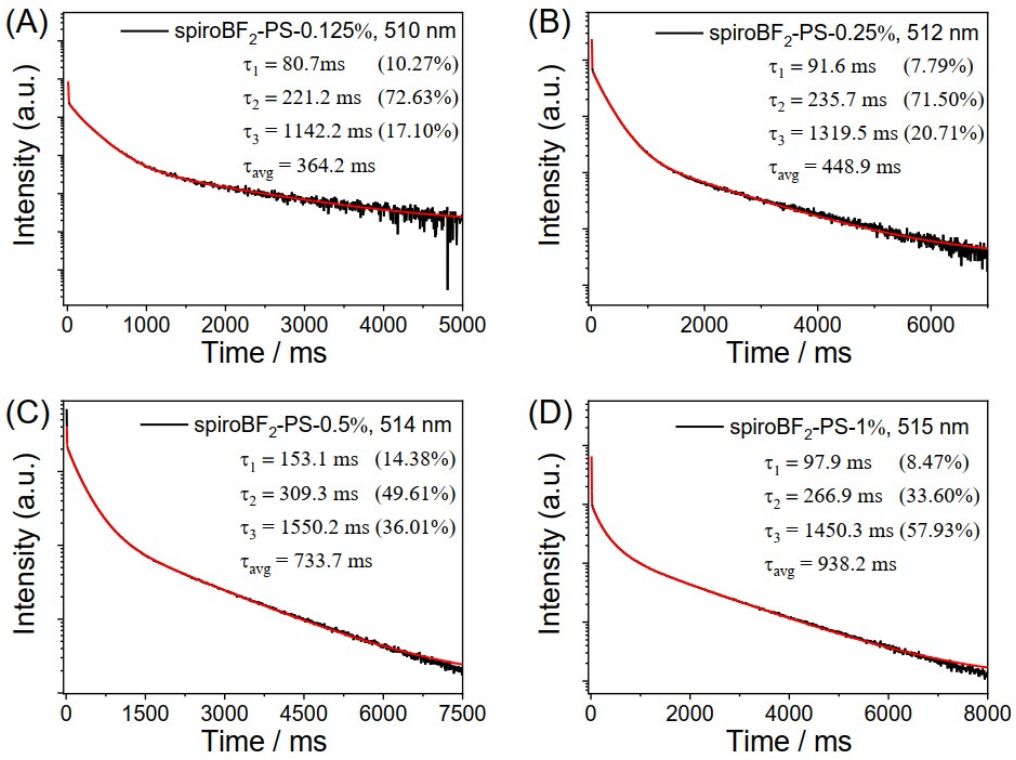

Figure S27. (A) Room-temperature emission decay of spiroBF$_2$-PS-0.125% samples excited at 328 nm and monitored at 510 nm. (B) Room-temperature emission decay of spiroBF$_2$-PS-0.25% samples excited at 361 nm and monitored at 512 nm. (C) Room-temperature emission decay of spiroBF$_2$-PS-0.5% samples excited at 356 nm and monitored at 514 nm. (D) Room-temperature emission decay of spiroBF$_2$-PS-1% samples excited at 373 nm and monitored at 515 nm.

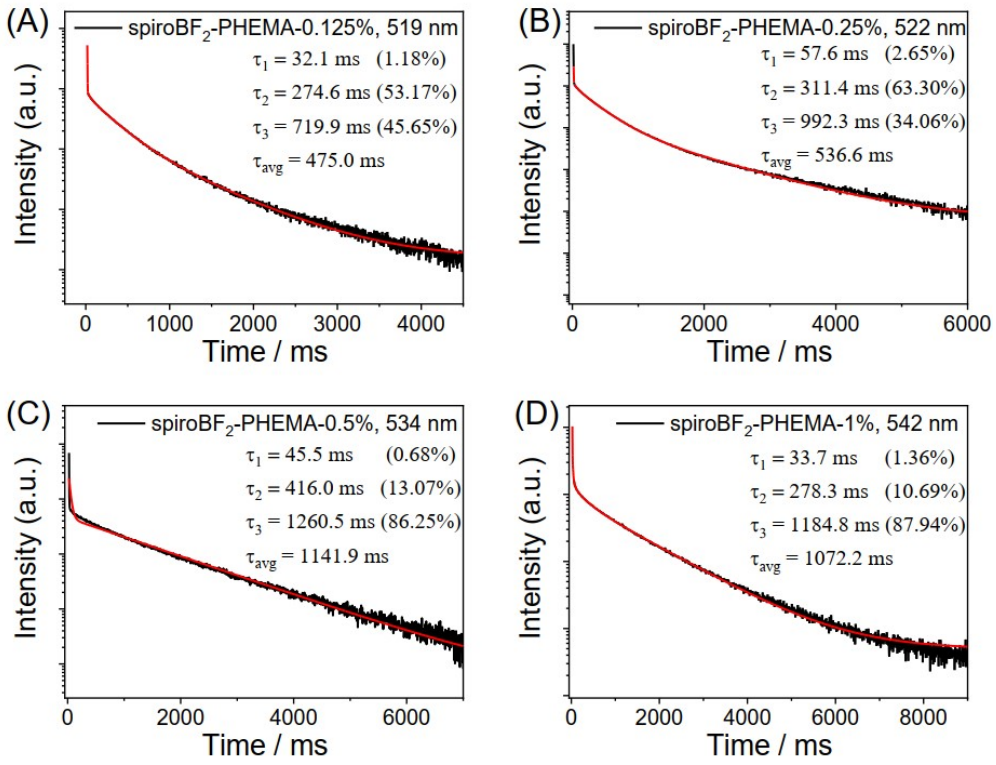

Figure S28. (A) Room-temperature emission decay of spiroBF$_2$-PHEMA-0.125% samples excited at 369 nm and monitored at 519 nm. (B) Room-temperature emission decay of spiroBF$_2$-PHEMA-0.25% samples excited at 372 nm and monitored at 522 nm. (C) Room-temperature emission decay of spiroBF$_2$-PHEMA-0.5% samples excited at 395 nm and monitored at 534 nm. (D) Room-temperature emission decay of spiroBF$_2$-PHEMA-1% samples excited at 428 nm and monitored at 542 nm.

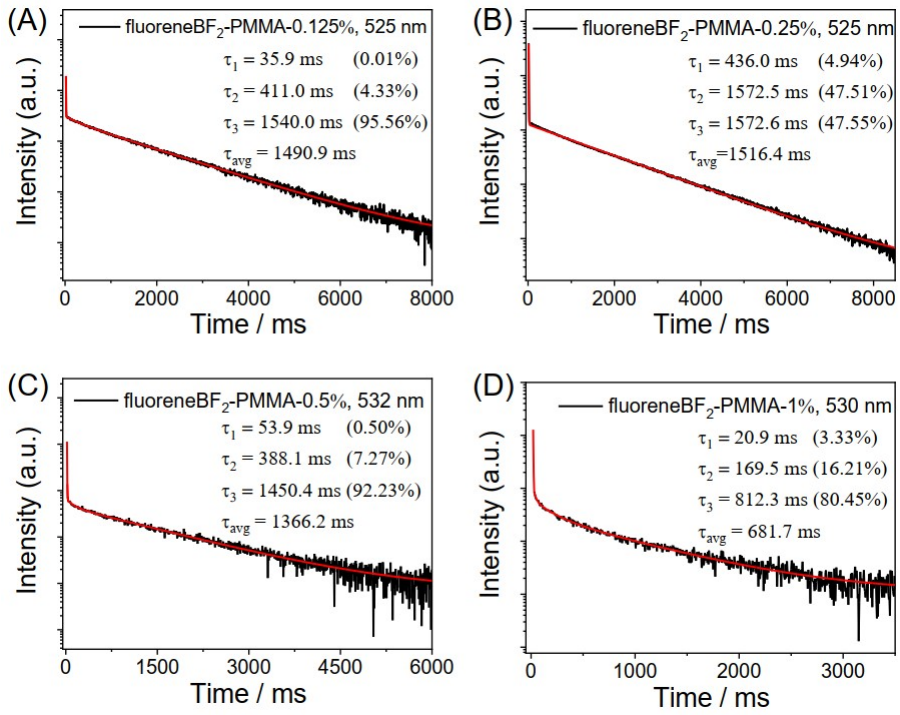

Figure S29. (A) Room-temperature emission decay of fluoreneBF$_2$-PMMA-0.125% samples excited at 387 nm and monitored at 525 nm. (B) Room-temperature emission decay of fluoreneBF$_2$-PMMA-0.25% samples excited at 388 nm and monitored at 525 nm. (C) Room-temperature emission decay of fluoreneBF$_2$-PMMA-0.5% samples excited at 387 nm and monitored at 532 nm. (D) Room-temperature emission decay of fluoreneBF$_2$-PMMA-1% samples excited at 384 nm and monitored at 530 nm.

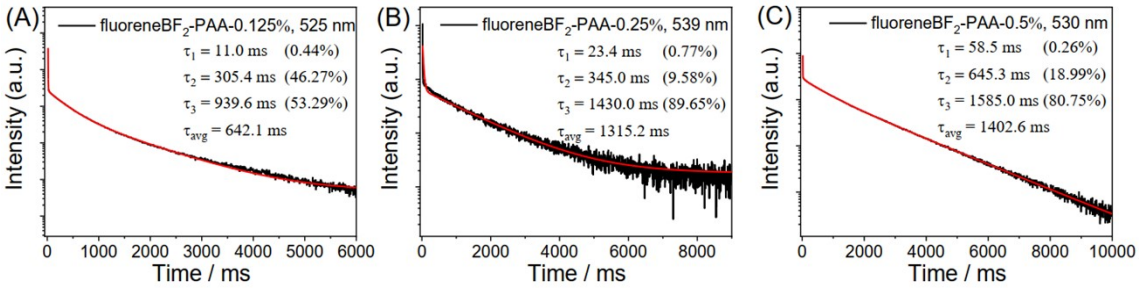

Figure S30. (A) Room-temperature emission decay of fluoreneBF$_2$-PAA-0.125% samples excited at 371 nm and monitored at 525 nm. (B) Room-temperature emission decay of fluoreneBF$_2$-PAA-0.25% samples excited at 402 nm and monitored at 539 nm. (C) Room-temperature emission decay of fluoreneBF$_2$-PAA-0.5% samples excited at 398 nm and monitored at 530 nm.

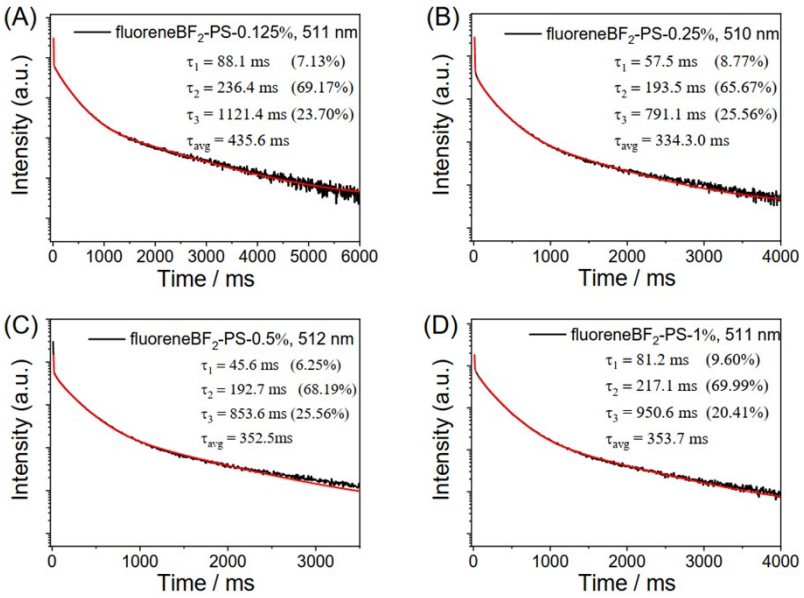

Figure S31. (A) Room-temperature emission decay of fluoreneBF$_2$-PS-0.125% samples excited at 364 nm and monitored at 511 nm. (B) Room-temperature emission decay of fluoreneBF$_2$-PS-0.25% samples excited at 365 nm and monitored at 510 nm. (C) Room-temperature emission decay of fluoreneBF$_2$-PS-0.5% samples excited at 365 nm and monitored at 512 nm. (D) Room-temperature emission decay of fluoreneBF$_2$-PS-1% samples excited at 366 nm and monitored at 511 nm.

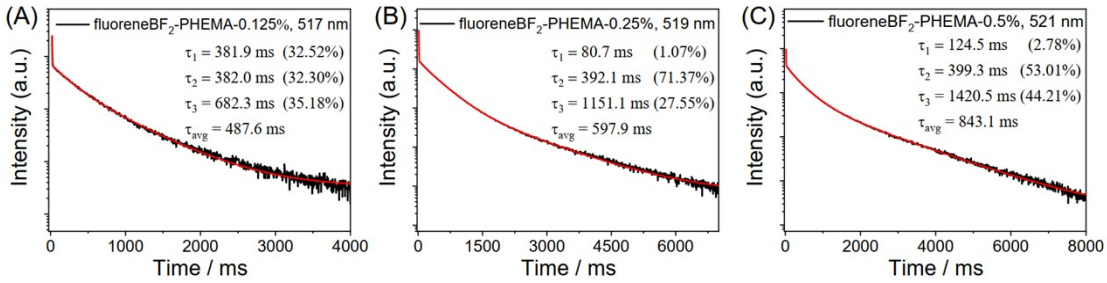

Figure S32. (A) Room-temperature emission decay of fluoreneBF$_2$-PHEMA-0.125% samples excited at 367 nm and monitored at 517 nm. (B) Room-temperature emission decay of fluoreneBF$_2$-PHEMA-0.25% samples excited at 374 nm and monitored at 519 nm. (C) Room-temperature emission decay of fluoreneBF$_2$-PHEMA-0.5% samples excited at 376 nm and monitored at 521 nm.

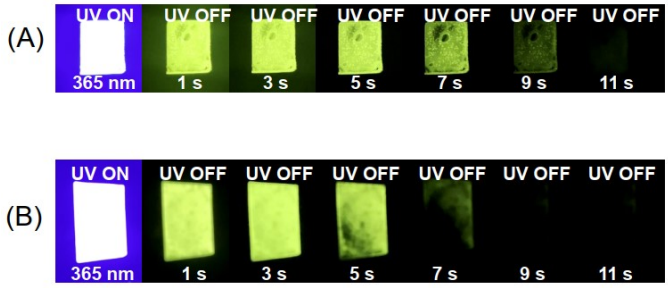

Figure S33. Photographs of (A) spiroBF$_2$-PMMA'-0.5% and (B) spiroBF$_2$-PS'-0.5% from commercial polymers prepared by solution casting technique under 365 nm UV lamp and after removal of UV lamp, and PMMA' (CM-211) and PS' (Mn=170,000) are commercially available.

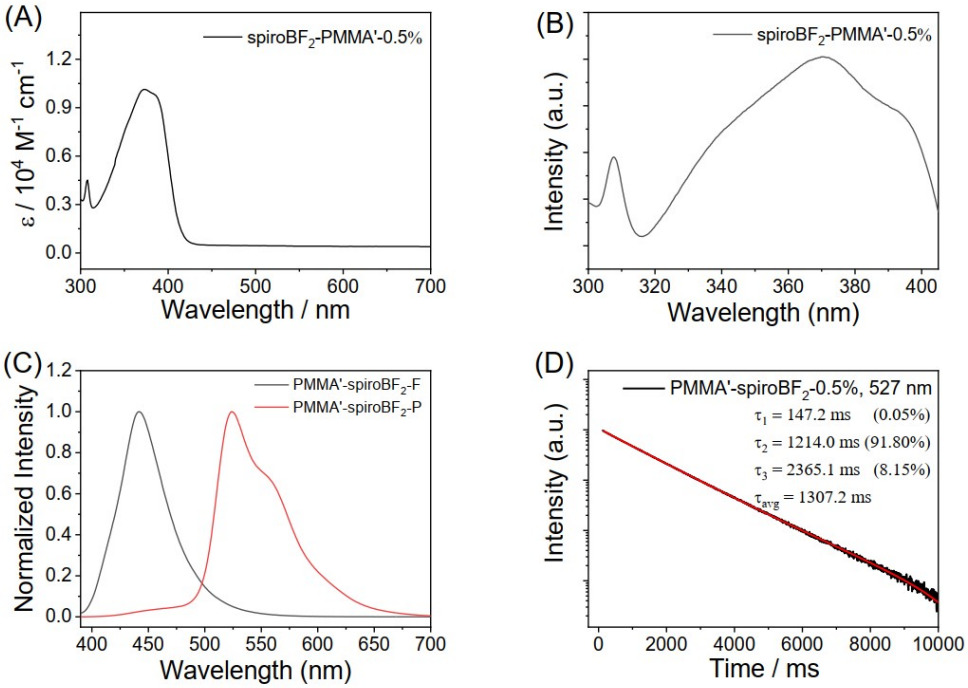

Figure S34. (A) UV-Vis spectra of spiroBF$_2$-PMMA'-0.5%. (B) Excitation spectra of spiroBF$_2$-PMMA'-0.5%. (C) Room-temperature fluorescence and phosphorescence spectra of spiroBF$_2$-PMMA'-0.5%. (D) Room-temperature emission decay of spiroBF$_2$-PMMA'-0.5% excited at 370 nm and monitored at 527 nm.

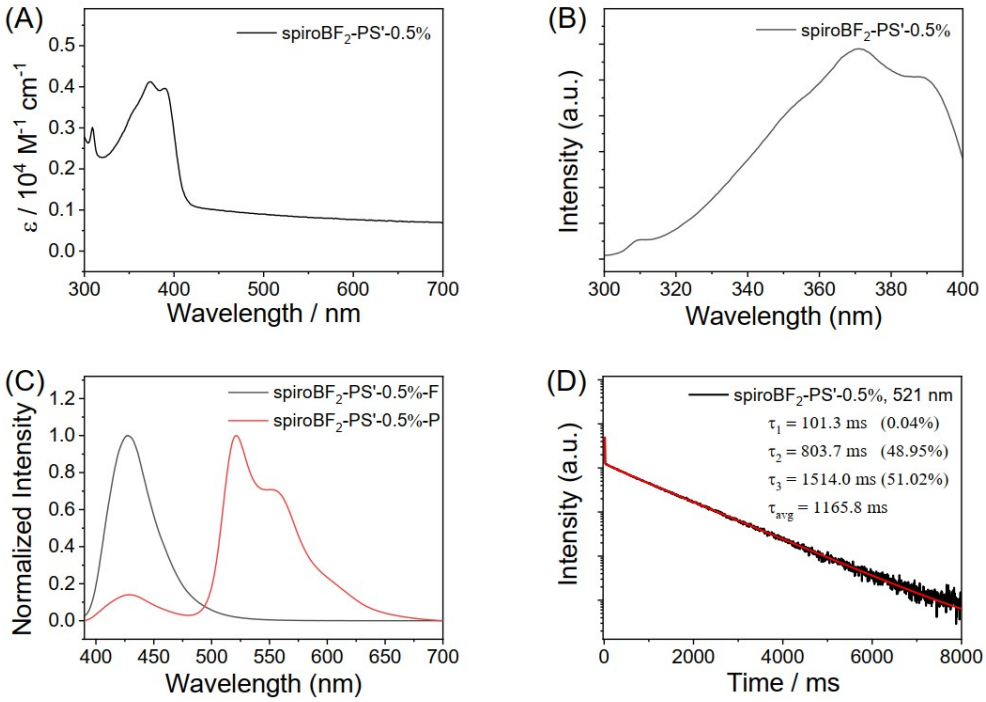

Figure S35. (A) UV-Vis spectra of spiroBF$_2$-PS'-0.5% (B) Excitation spectra of spiroBF$_2$-PS'-0.5%. (C) Room-temperature fluorescence and phosphorescence spectra of spiroBF$_2$-PS'-0.5%. (D) Room-temperature emission decay of spiroBF$_2$-PS'-0.5% excited at 369 nm and monitored at 521 nm.

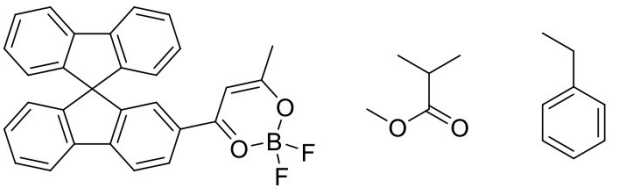

Figure S36. Dipole moments of spiroBF$_2$'s S_1 state, PMMA's repeating unit, and PS's repeating unit. TD-DFT calculations (B3LYP/aug-cc-pVTZ) showed that spiroBF$_2$ in its S_1 state has a dipole moment of 15.9 D. The strength of dipole-dipole interactions between spiroBF$_2$'s S_1 states and organic matrices would increase as the dipole moments of the organic matrices increase. To estimate the dipole moments of the polymeric matrices, DFT calculations on the repeating units of the polymeric matrices have been performed. The dipole moments of PS are smaller than those of PMMA, while PS still possesses non-negligible dipole moments. According to the reported studies (*J. Am. Chem. Soc.* **2017**, *139*, 4042), a reduction in ΔE_{ST} on the order of 0.05 eV can increase k_{ISC} by approximately 1 order of magnitude. These studies further support that the polymeric matrices with dipole moments can interact with and perturb the singlet excited states of luminescent dopants via dipole-dipole interactions, reduce ΔE_{ST} and consequently enhance ISC of spiroBF$_2$ excited states.

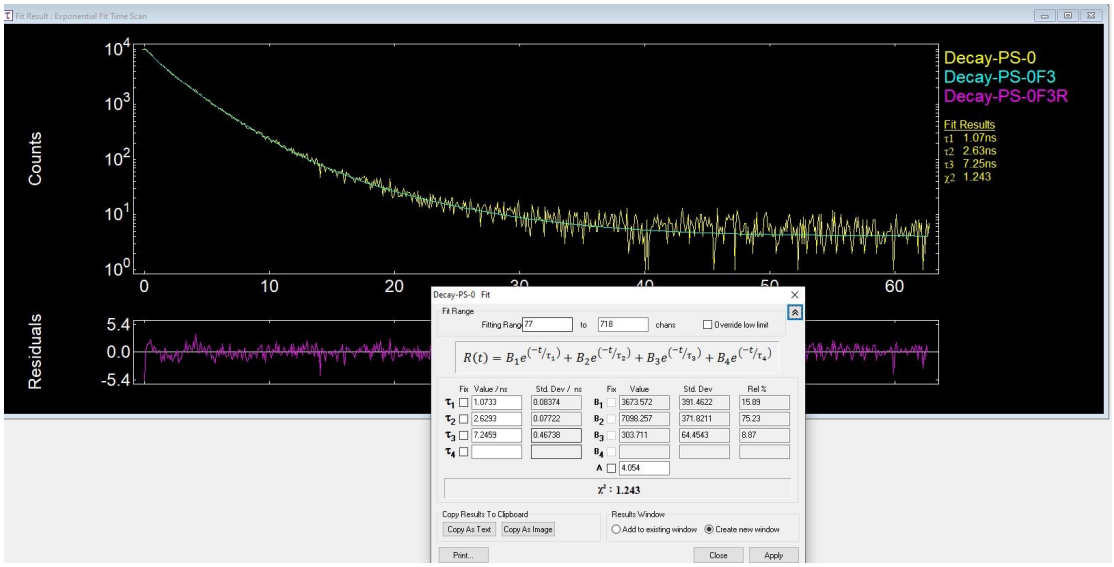

Figure S37. Room-temperature emission decay of spiroBF$_2$-PS-0.5% materials monitored at 428 nm.

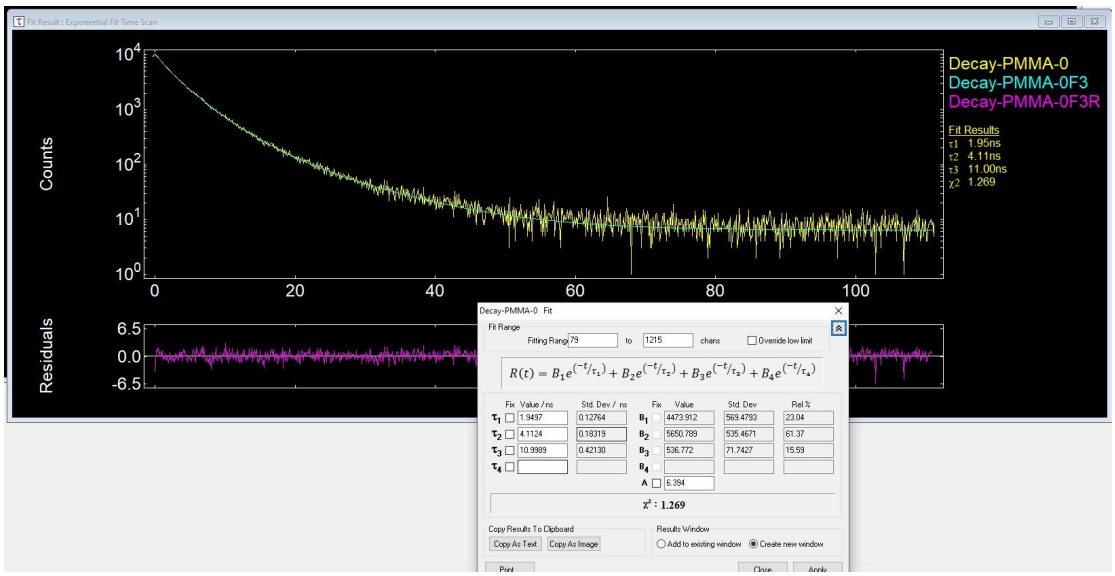

Figure S38. Room-temperature emission decay of spiroBF$_2$-PMMA-0.5% materials monitored at 434 nm.

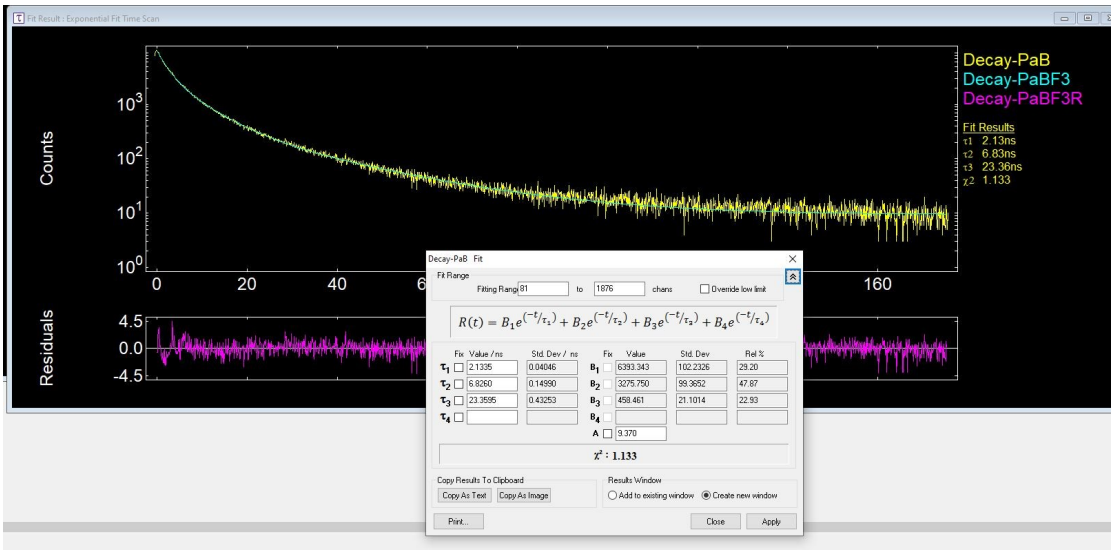

Figure S39. Room-temperature emission decay of spiroBF$_2$-PhB-0.5% materials monitored at 451 nm.

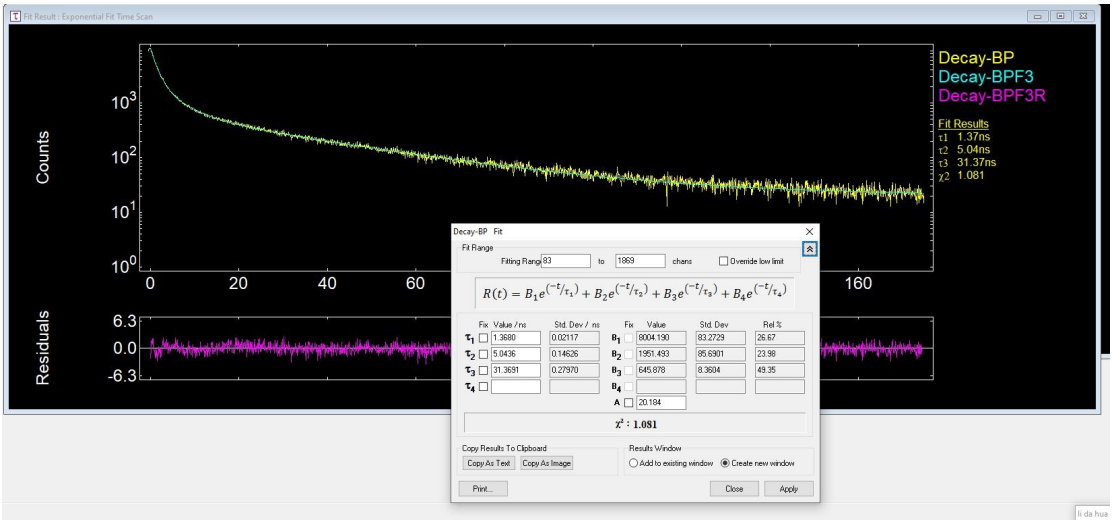

Figure S40. Room-temperature emission decay of spiroBF$_2$-BP-0.5% materials monitored at 465 nm.

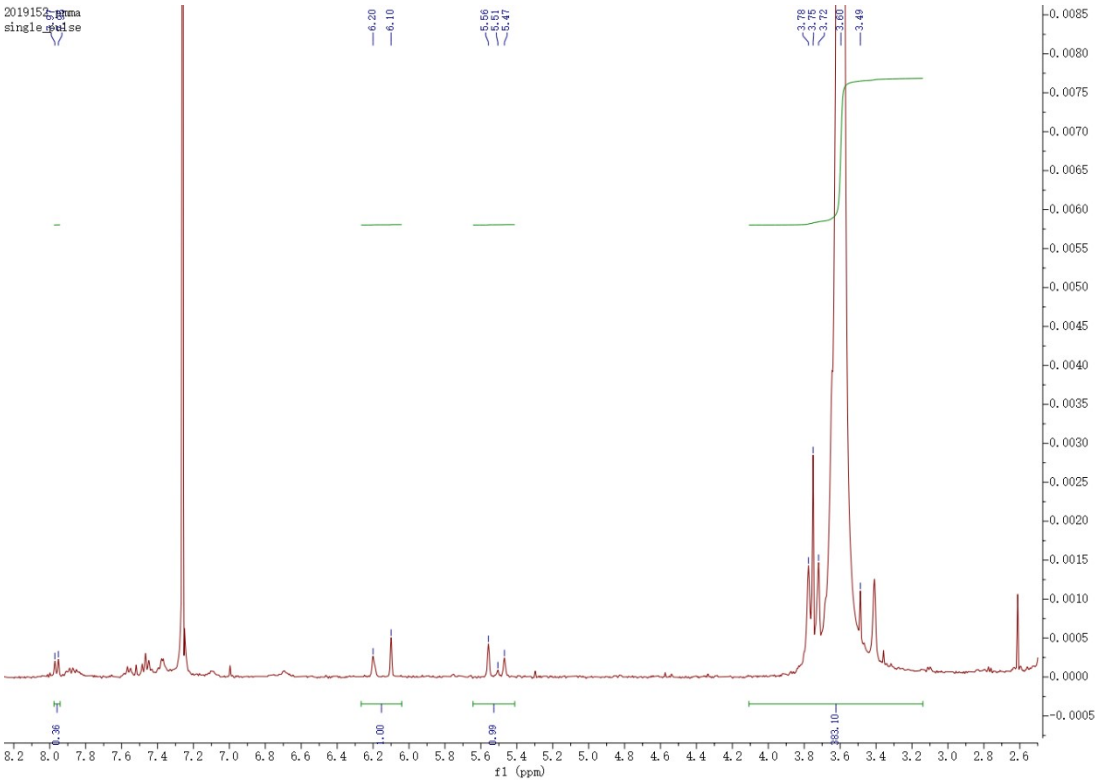

Figure S41. ^{1}H NMR spectra of spiroBF$_2$-PMMA-0.5% materials. In the case of spiroBF$_2$-PMMA-0.5%, it has been found that monomer conversion efficiency of the photopolymerization is close to unity as estimated by ^{1}H NMR; the concentration of the residual monomers is less than 0.8%.

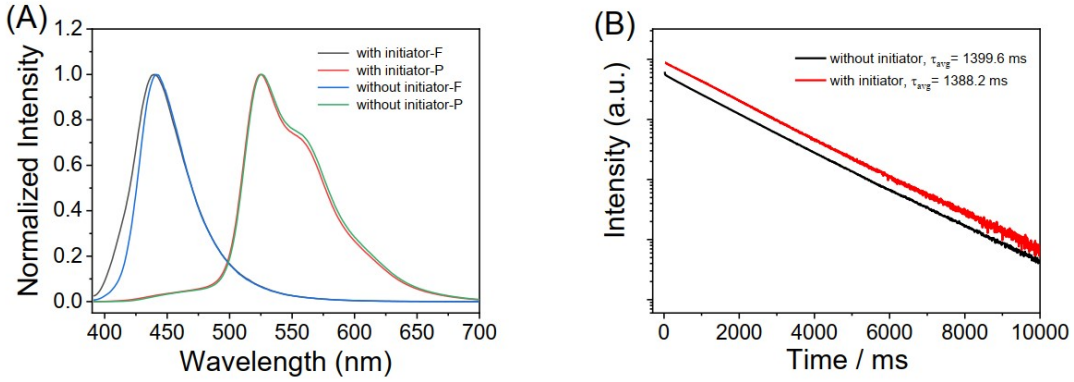

Figure S42. (A) Room-temperature fluorescence and phosphorescence spectra of two samples of spiroBF$_2$-PMMA-0.5% with and without photoinitiator (0.2%) in degassed conditions. (B) Room-temperature emission decay of two samples of spiroBF$_2$-PMMA-0.5% with and without initiator in degassed conditions (excited at 371 nm and monitored at 525 nm).

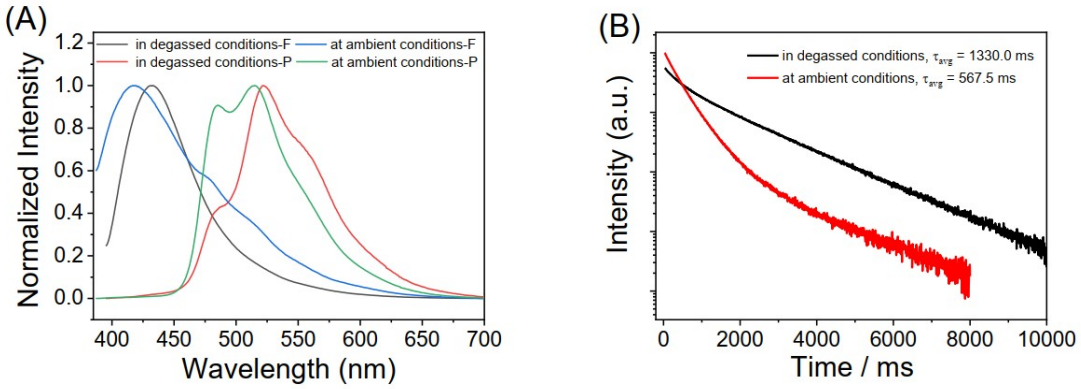

Figure S43. (A) Room-temperature fluorescence and phosphorescence spectra of spiroBF$_2$-PMMA-0.5% measured at ambient conditions and in degassed conditions. (B) Room-temperature emission decay of spiroBF$_2$-PMMA-0.5% measured at ambient conditions and in degassed conditions; the former is excited by 367 nm and monitored by 515 nm, while the latter is excited by 375 nm and monitored by 522 nm. The spiroBF$_2$-PMMA-0.5% samples have been found to show RTP lifetimes of 1330.0 ms under degassed conditions, much longer than those under ambient conditions (567.5 ms). These suggest that oxygen can diffuse into PMMA matrices and quenching RTP of spiroBF$_2$ to a certain extent. In the present study, the rigid microenvironments provided by the glassy polymer matrices can restrict the nonradiative deactivation of BF$_2$bdk triplets and protect the triplets from oxygen quenching to a certain extent.

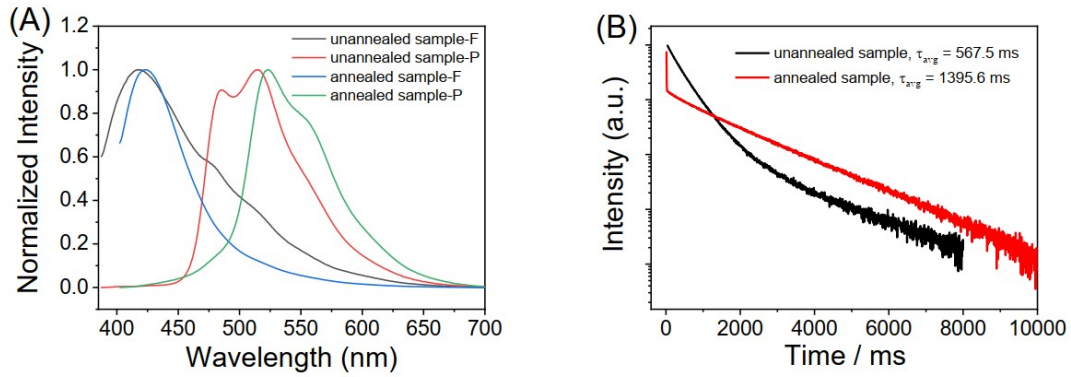

Figure S44. (A) Room-temperature fluorescence and phosphorescence spectra of spiroBF$_2$-PMMA-0.5% before and after thermal annealing. (B) Room-temperature emission decay of spiroBF$_2$-PMMA-0.5% before and after thermal annealing; the former is excited by 367 nm and monitored by 515 nm, while the latter is excited by 382 nm and monitored by 523 nm.

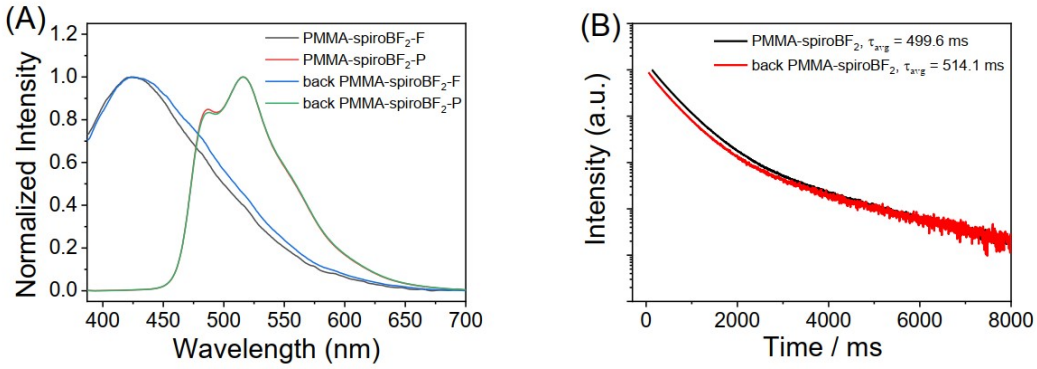

Figure S45. (A) Room-temperature fluorescence and phosphorescence spectra on both sides of reconstituted spiroBF$_2$-PMMA-0.5%. (B) Room-temperature emission decay on both sides of spiroBF$_2$-PMMA-0.5% excited by 367 nm and monitored by 515 nm.

Table S1. Cartesian coordinates of the optimized ground-state geometry of spiroBF$_2$

F	7.37508086	8.19163832	7.01178143
F	7.37075649	8.69827597	9.25838091
O	6.48204221	10.22987298	7.73460309
O	5.37893226	8.08121622	8.21060426
C	5.33206743	12.27070253	7.66365068
H	5.72190568	12.48557213	6.66696574
H	4.33706260	12.69713099	7.76751592
H	6.00725408	12.74343864	8.38036641
C	5.33527682	10.79621578	7.88899386
C	4.19438984	10.08956043	8.22319245
H	3.26608333	10.62007050	8.33901746
C	4.25715660	8.70180483	8.35420780
C	3.10313119	7.85756799	8.63101563
C	1.82499723	8.38685015	8.82361340
H	1.66743513	9.45402656	8.77039940
C	0.75207554	7.56250757	9.08280240
H	-0.23038503	7.98894339	9.23392353
C	0.95168377	6.19490315	9.14608488
C	0.03149023	5.10596751	9.39745822
C	-1.32974607	5.10722697	9.65173285
H	-1.88900093	6.03346520	9.68192157
C	-1.97253966	3.90108913	9.86792362
H	-3.03524188	3.88044384	10.07172611
C	-1.25663685	2.70967119	9.82560446
H	-1.76942009	1.77196930	9.99538241
C	0.10639462	2.71573782	9.56760566
H	0.65334082	1.78279634	9.53638002
C	0.74509991	3.91443144	9.35285686
C	2.19877293	4.16309248	9.05412585
C	2.22048784	5.66245996	8.94981701
C	3.28541668	6.47511535	8.69761117
H	4.27546335	6.07194754	8.54598758
C	3.14269990	3.59651059	10.08627495
C	3.18967199	3.86336341	11.43460929
H	2.49923116	4.56251384	11.88860775
C	4.13735466	3.22071452	12.21944585
H	4.18691747	3.42069521	13.28168900

C	5.02588423	2.31944767	11.64623491
H	5.76131938	1.82441020	12.26721493
C	4.97621121	2.05338039	10.28692780
H	5.67346069	1.35168883	9.84784360
C	4.02951694	2.69632339	9.51021059
C	3.74513067	2.61713516	8.08562247
C	4.33771413	1.88009118	7.07652027
H	5.16633786	1.21602198	7.28593275
C	3.85907658	2.00267251	5.78134657
H	4.31638909	1.43656316	4.98009948
C	2.79474818	2.85137208	5.50355198
H	2.42866218	2.93788163	4.48886693
C	2.20334800	3.58770169	6.52026262
H	1.37338749	4.24603832	6.29760379
C	2.68389445	3.46697131	7.80282952
B	6.71421667	8.76979047	8.05605205

Table S2. Cartesian coordinates of the optimized ground-state geometry of fluoreneBF_2

F	4.37565528	-2.04853807	-1.10478005
O	2.65826314	-0.78083899	-0.15785599
O	5.00361430	-0.02572791	-0.11506298
C	-2.50597623	-1.35592110	0.03571803
C	-3.75898633	-0.48162005	0.01604202
C	-5.09410441	-0.87035109	0.03006603
H	-5.36890642	-1.92129517	0.05871303
C	-6.08957450	0.11259497	0.00692802
H	-7.13509360	-0.18107507	0.01776602
C	-5.75315647	1.47076507	-0.02996498
H	-6.53945856	2.21944611	-0.04746398
C	-4.41630940	1.86894411	-0.04440998
H	-4.15791739	2.92372419	-0.07309998
C	-3.42234531	0.88696905	-0.02140998
C	-1.96282221	1.00322208	-0.02910898
C	-1.13195516	2.12732617	-0.06357398
H	-1.54938221	3.12912924	-0.09674098
C	0.24693194	1.94865617	-0.06041798
H	0.88619997	2.82312724	-0.10320298
C	0.81275799	0.65848409	-0.02399498
C	-0.03541406	-0.46933300	0.00345702
H	0.41295999	-1.45617907	0.02844403
C	-1.40766316	-0.29396201	0.00329502
C	-2.43729321	-2.27382716	-1.20591107
H	-2.48921022	-1.69253012	-2.13066313
H	-3.26806026	-2.98683722	-1.20277606
H	-1.50392213	-2.84553619	-1.21228606
C	2.26930210	0.44717209	-0.01588898
C	3.20962015	1.48158618	0.12270203
H	2.90125112	2.50605724	0.26280804
C	4.56481926	1.18231117	0.03282203
C	5.62930434	2.23665025	0.08263103
B	4.10251025	-1.24209802	-0.04246698
F	4.26484627	-1.82862806	1.18171811
C	-2.42935821	-2.20498116	1.32495312
H	-2.47562422	-1.57431611	2.21710418
H	-3.25998526	-2.91698722	1.36580212
H	-1.49588813	-2.77573719	1.35637212
H	6.30081338	2.03501525	0.92349109
H	6.23326735	2.18478326	-0.82891704
H	5.21020928	3.23861632	0.18429304

Supporting References

(S1) Neese, F. (2018), Software update: the ORCA program system, version 4.0. WIREs Comput Mol Sci, 8: e1327. doi:10.1002/wcms.1327.

(S2) A. D. Becke, “Density-functional exchange-energy approximation with correct asymptotic-behavior,” Phys. Rev. A, 38 (1988) 3098-100.

(S3) C. Lee, W. Yang, and R. G. Parr, “Development of the Colle-Salvetti correlation-energy formula into a functional of the electron density,” Phys. Rev. B, 37 (1988) 785-89.

(S4) B. Miehlich, A. Savin, H. Stoll, and H. Preuss, “Results obtained with the correlation-energy density functionals of Becke and Lee, Yang and Parr,” Chem. Phys. Lett., 157 (1989) 200-06.

(S5) F. Weigend and R. Ahlrichs, Phys. Chem. Chem. Phys. 7, 3297 (2005).

(S6) Tian Lu, Feiwu Chen, J. Comput. Chem., 33, 580-592 (2012).

(S7) Humphrey, W., Dalke, A. and Schulten, K., `VMD – Visual Molecular Dynamics', J. Molec. Graphics 1996, 14.1, 33-38.